Computational Fluid Dynamic simulation of a high-throughput catalytic fixed-bed reactor for total oxidation of methane

*Mohammad Rusydi Fatahillah[a], Reza Monjezi[a], Yi Ouyang[a], Joris W. Thybaut[a], Dirk Poelman[b], and Geraldine J. Heynderickx[a]**

[a] Laboratory for Chemical Technology, Department of Materials, Textiles, and Chemical Engineering, Ghent University, Technologiepark 125, B-9052 Ghent, Belgium

[b] LumiLab, Department of Solid State Sciences, Ghent University, Krijgslaan 281–S1, 9000 Ghent, Belgium

* Corresponding author: Geraldine.Heynderickx@UGent.be

Abstract

This paper presents a 2D Computational Fluid Dynamics (CFD) study to investigate the performance of our high-throughput fixed-bed reactor used for the total oxidation of diluted volatile organic compounds (VOCs) in a continuous gas stream. The CFD model, based on a porous media and a power law kinetic model, is validated by comparing the calculated and experimentally determined conversion of methane, the selected VOC, over the β-cyclodextrin-Cu/Hydroxyapatite catalyst for different operating conditions. The CFD model captures the effect of varying partial pressures of methane and oxygen on the methane conversion at various space time and temperature. Overall, simulation results qualitatively agree with experimental data within an average deviation of 17%. Analysis of the flow field, calculated using CFD, suggests that the reactor behavior resembles that of an ideal plug flow reactor. The findings set out the lines for creating a simplified 1D model of the high-throughput reactor in our future research.

1. Introduction

As most people spend 70% to 90% of their time indoors,[1] there is a growing attention for the effects of indoor air quality on health and well-being.[2-3] Volatile Organic Compounds (VOCs) are major indoor air pollutants generated from various emission sources, including cooking, heating, and common household items.[2, 4-5] Many VOCs are considered hazardous as they may cause impairment of the nervous system, respiratory diseases, and cancer.[6-8]

Several technologies have been identified to reduce indoor VOC pollutants,[9-10] including heterogeneous catalytic oxidation. Catalytic oxidation is a promising technology, enabling nearly complete conversion of dilute VOCs into less harmful products at low operating temperatures.[5, 11] The process is versatile, as it is possible to use a range of catalysts that can be prepared to meet the characteristics of the VOCs.[8, 12] Consequently, catalytic oxidation offers an excellent opportunity to design tailor-made catalysts that effectively reduce VOCs emission indoors.

Research into the catalytic oxidation of numerous VOCs has been conducted using various catalysts, as documented in several review articles.[8, 11-14] However, in-depth experimental studies, including kinetic modeling, are still required to find the best catalyst to remove selected VOCs. Choudhary and Deshmukh investigated the total oxidation of diluted propane and methyl ethyl ketone over a Cr-doped ZrO_2 catalyst in a continuous fixed-bed micro-reactor.[15] They evaluated two kinetic models using a power law and a Mars-Van Krevelen kinetic expression. The Mars-Van Krevelen redox model was found to give a better fit than the power law model for both propane and methyl ethyl ketone. The total catalytic oxidation of methane over supported CuO catalysts at 633 – 933 K was investigated by Águila et al.[16] The effect of adding reaction products to the gas inlet flow on methane conversion was also studied.[16] Heynderickx et al. presented the results for the total oxidation of propane in a conventional fixed-bed reactor, operating at 543 – 648 K, using a commercial $CuO\text{-}CeO_2/\gamma\text{-}Al_2O_3$ catalyst.[17] These authors constructed a comprehensive kinetic model using a mechanistic approach, i.e., based on the elementary reaction step in the reaction mechanism.[17] They concluded that a Langmuir-Hinshelwood type of rate equation describes the oxidation of propane adequately.[17]

Several researchers investigated the VOCs total oxidation, but only few of those[18-21] combined a hydrodynamic study of the applied reactor with reaction rate calculations. The use of reaction rate is essential for determining the proper size of a reactor, thus, offering opportunities to minimize capital costs without sacrificing reactor performance. The lack of combining hydrodynamics and reaction chemistry can be effectively tackled by performing reactive flow Computational Fluid Dynamics (CFD) simulations. CFD is a powerful tool to model reactor hydrodynamics accounting for the reactions taking place. Once the combined model is validated, it can be used to understand reactor behavior, to optimize operating conditions and reactor geometry, to design new reactor technology, or to scale up the process.[22] Although CFD modeling was already demonstrated to be applicable for various reactor geometries, including a gas-solid vortex reactor,[23] a lateral flow reactor,[24] and a fixed-bed reactor,[25] there is hardly any report on CFD modeling of catalytic VOC oxidation reactors. Choi and Yi performed CFD simulations of a three-bed regenerative thermal oxidizer treating a gas stream containing benzene, toluene, and xylene to evaluate the destruction of the VOCs as well as assess the flow field and temperature distribution within the reactor.[18] Odiba et al. used CFD to simulate a microreactor comprising eleven parallel channels with a square cross-section to remove propane in order to assist in designing a new reactor.[21] In this reactor, the catalyst was uniformly deposited on the channel walls as a thin and homogeneous layer. A hybrid model combining CFD with an Artificial Neural Network (ANN) approach for kinetic modeling was developed by Sokhansanj et al. to remove benzene and toluene.[19] In this study, the CFD was utilized to predict and study the behavior of the catalytic reactor in an efficient manner. They used a cobalt-based Metal Organic Framework (MOF) on activated carbon as a catalyst in a tubular fixed-bed reactor.[19] Niaei et al. developed a 3D CFD model including Mars-Van Krevelen kinetics to simulate the catalytic oxidation of ethyl acetate.[20] The CFD study was valuable to predict the flow field and temperature distribution as well as to investigate the reactor behavior without the need to carry out extended experimental works.[20] They used a tubular reactor characterized by a tube-to-particle diameter ratio of two, containing 20 spherical solid particles of Cr-HZSM-5 catalyst.

The present work aims at developing a CFD model that describes the performance of a β-cyclodextrin-Cu/Hydroxyapatite (βCD-Cu/HAP) catalyst for the total oxidation of methane, a prominent VOC, in a high-throughput fixed-bed reactor exclusively designed to screen and develop new catalysts.[26-29] The βCD-Cu/HAP catalyst is selected in this study as the incorporation of β-cyclodextrin enhances the catalytic performance of CuO supported HAP due to the enhanced Cu dispersion, as described by Ibrahim et al.[30] The calculated methane conversion is compared to experimental data gathered over a wide range of operating conditions, including space time, reaction temperature, and partial pressure of both methane and oxygen.

2. Experimental setup

The High-Throughput Kinetic Screening (HTK-S) reactor is a fixed bed reactor built as an efficient setup to develop new catalysts. The HTK-S is comprehensively described in the work of Van der Borght et al.[27] Experimental data obtained in the HTK-S allows the determination of intrinsic kinetics.[29] The HTK-S setup comprises three main parts: a feed section, a reactor section, and an analysis section, as illustrated in Figure 1. The feed section is designed to mix several gases, to control the volumetric gas flow, and to ensure a uniform gas distribution from a single line to four parallel lines of fixed-bed reactors.

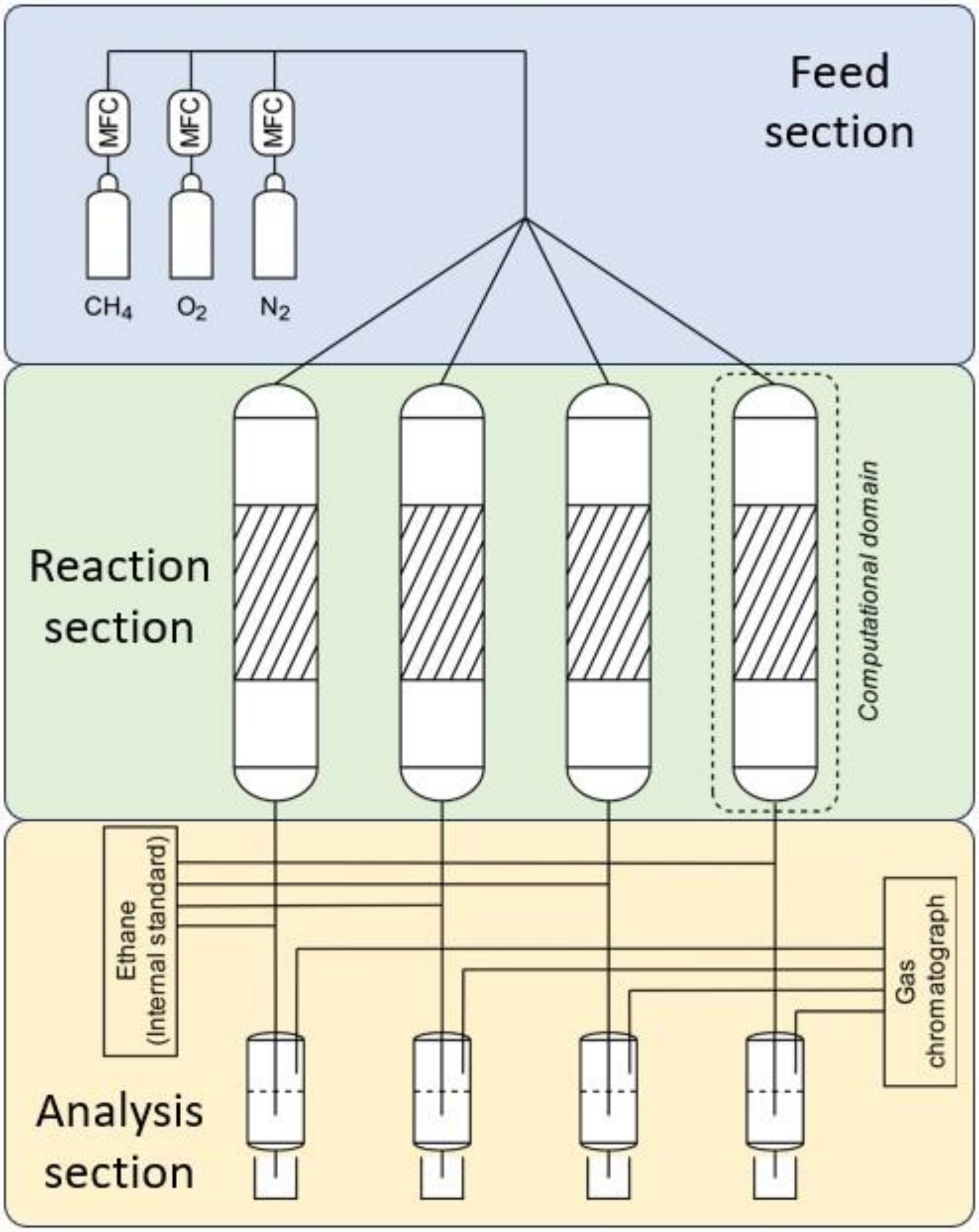

Figure 1. Schematic diagram of the HTK-S experimental setup

The computational domain covers just one of those four identical fixed-bed reactors, as shown in Figure 2. In summary, the fixed-bed reactor is 850 mm long and has an inner diameter of 2.2 mm, resulting in a high length-over-diameter ratio. The reactor is assumed to have a uniform bed porosity of 0.4.[31] The reactor section is equipped with a back-pressure valve to regulate the reactor pressure and an electric oven to control the reaction temperature. The effluent composition is analyzed using a Gas Chromatograph (Thermo Fisher Scientific) equipped with a thermal conductivity detector. The methane conversions are calculated and used as validation data for the proposed CFD model.

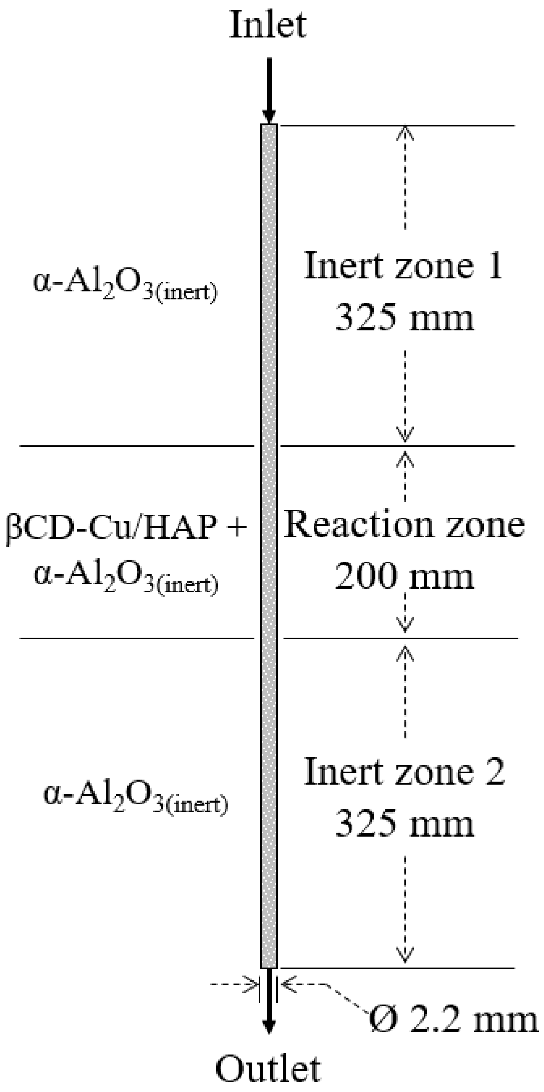

Figure 2. Computational domain of the high-throughput catalytic fixed-bed reactor. Total height of a reactor tube is 850 mm.

Table 1 provides detailed information about operating and boundary conditions. Several sets of experiments at different process parameters are carried out while keeping some parameters constant at all times, such as the total gas inlet volumetric flow rate (5.1 NL/h), the combined weight of catalyst and inert (1.3 grams combined), and the outlet gas pressure (500 kPag).

The experiments are varied by imposing different process parameters, including space time, temperature, and partial pressure of methane and oxygen. Firstly, the amount of catalyst in the middle (or reaction) zone of the fixed-bed reactor (see Table 1) is changed per experiment to vary the space time. For example, when a catalyst mass of 0.073 and 0.200 grams is specified for a methane partial pressure of 2.91 kPa, the space time equals 196 and 535 $\mathrm{kgcat{\cdot}s{\cdot}mol_{CH_4}^{-1}}$, respectively. Given the design of the HTK-S reactor setup, the weight of the catalyst in the reactor is limited to 0.2 grams, needed to disregard a radial temperature gradient in the catalyst bed. The lowest amount of catalyst required to achieve a notable methane conversion corresponds to 0.073 grams. The catalyst weights of 0.113 and 0.153 grams are selected to realize a well-distributed space time interval, as determined by the minimum and maximum catalyst weight. Remark that for a given space time, the amount of inert in the reaction zone is calculated by subtracting the specified amount of catalyst from the total weight of 1.3 grams. The catalyst used in the presented study is prepared according to the method described by the work of Ibrahim et al.[30]

Secondly, when the methane partial pressure is set at 2.91, 4.52, and 7.97 kPa, the oxygen partial pressure is kept constant at 32.65 kPa, and the total outlet gas pressure is kept at 500 kPag by the back-pressure valve. Similarly, when the oxygen partial pressure has set values of 16.64 and 32.65 kPa, the methane partial pressure is kept constant at 2.91 kPa, and the N_2 partial pressure is adapted to maintain the imposed gas pressure at the outlet. Changing partial pressures is done by adapting each species' inlet volumetric flow rate. Finally, the reactor wall temperature, crucial for determining the reaction temperature, is determined by the oven set-point temperature and varies throughout the experimental work.

Table 1. Overview of operating conditions and boundary conditions

Solid bed properties	
Catalyst	βCD-Cu/HAP
Inert material	α-Al_2O_3
Total weight catalyst + inert	1.3 g (all experiments)
Catalyst weight	0.073, 0.113, 0.153, 0.200 g
Mean particle diameter	0.125 mm
Bed porosity	0.4
Particle density	3,900 kg·m^{-3}
Heat capacity	1,255 J·kg^{-1}·K^{-1}
Heat conductivity	7 W·m^{-1}·K^{-1}
Gas feed	
Composition	2.91, 4.57, 7.97 kPa CH_4 16.64, 32.65 kPa O_2 N_2 as balance gas
Density calculation	Ideal gas
Transport and thermophysical properties	Kinetic gas theory
Viscous model	Laminar

Boundary conditions (all experiments)	
Inlet (mass flow rate inlet)	5.1 NL/hour gas at 293 K
Outlet (pressure outlet)	500 kPa_g
Walls	No slip condition
Wall thickness	4.25 mm
Wall temperatures	623, 648, 673, 698, 723 K

3. Model description

3.1. Governing equations

The HTK-S fixed-bed reactor is modeled as a porous medium with an isotropic bed porosity in a 2D axisymmetric geometry. This model considers both the gas and solid phase to be a continuous phase.[32] Work by Gao et al. confirms that the 2D porous media model performs well in the CFD simulation of a fixed-bed reactor.[25] The use of this model to simulate the catalytic fixed-bed reactors was already validated for different processes, including diethyl oxalate formation from carbon monoxide,[25] butylene oxidative dehydrogenation,[26] and methanol to olefins.[33] Other research groups have also successfully used this approach.[34-36] Additionally, the high tube-to-particle diameter ratio justifies the use of the porous media approach.[37-41] The disadvantage of the porous media model is that the calculated gas velocity is not particle-resolved.[37, 41]

The conservation and constitutive equations that contribute to the porous media model used for the CFD simulations are listed in Table 2. They include the gas-phase continuity equation (Eq. 1), gas-phase momentum equation (Eq. 2), energy equation (Eq. 3), and the species transport model equation (Eq. 4). The simulations are carried out using the commercial CFD software package ANSYS FLUENT 2021 R2 (steady-state pressure-based solver with double precision). The coupled scheme is selected to account for the pressure-velocity coupling. The second-order upwind scheme is chosen for the spatial discretization of computed variables to ensure reasonable accuracy. The convergence criteria for the iterative calculations include residuals that are set to 10^{-5} for the continuity and species transport equations and set to 10^{-6} for the other equations.

In the porous media model applied in this work, a source term is added to the gas phase momentum equation, introducing the effect of the solid bed.[42] This source term is calculated in Eq. 7, with K_{perm} representing the permeability of 4.6×10^{-11} m^2 and K_{loss} the loss coefficient of 1×10^5 m^{-1}. The permeability contribution in Eq. 7 is equivalent to Darcy's law, where the pressure drop in the porous media is proportional to the gas velocity. The inertial loss contribution in Eq. 7 accounts for a loss coefficient per unit length in the flow direction. This allows to specify the pressure drop as a function of the dynamic head. The estimation of the gas-phase pressure drop is taken from the Ergun equation for flow through a packed bed (Eq. 8),[43] which is assumed to be reliable for the HTK-S reactor.[44]

The energy equation (Eq. 3) is solved to obtain the temperature field.[42] The porous media model is applied assuming thermal equilibrium conditions, where the gas and solid phases are considered to have the same temperature. This choice is justified due to the high thermal conductivity of α-Al_2O_3 (the inert) with a relatively small mean particle diameter of 0.125 mm in the solid phase. The thermal equilibrium assumption is expressed in the energy equation by using the effective thermal conductivity of the gas and solid phase. A similar assumption of thermal equilibrium using effective conductivity is also adopted by other researchers using the porous media model.[35, 45] In this work, the approach is also justified by the low total gas mass flow rate (1.7 × 10^{-6} kg/s) and the limited contribution of reaction enthalpy, as the methane concentration in the gas stream is only 0.6% mol/mol.

Table 2. Overview of conservation equations and constitutive equations of the porous media model

---

Gas phase continuity equation (1)

$$\nabla\left(\varepsilon\rho_g\vec{u}\right) = 0$$

Gas phase momentum equation (2)

$$\nabla\left(\varepsilon\rho_g\vec{u}\vec{u}\right) = -\varepsilon\,\nabla p + \nabla\varepsilon\,\bar{\bar{\tau}} + \vec{S}_{PM}$$

Energy equation (3)

$$\nabla\left[\varepsilon\,\vec{u}\left(\rho_g E_g + p\right)\right] = \nabla\left[\left(\varepsilon\lambda_g + (1-\varepsilon)\lambda_s\right)\nabla T - \sum\left(h_i\vec{J_i}\right) + \bar{\bar{\tau}}\,\vec{u}\right] - \sum\frac{h_i^f}{M_i}\,R_i$$

Species transport equation (4)

$$\nabla\left(\varepsilon\rho_g\vec{u}Y_i\right) = -\nabla\vec{J}_i + R_i$$

Gas phase equation of state (5)

$$p = \frac{\rho_g R_{gas} T}{M}$$

Gas phase stress tensor (6)

$$\bar{\bar{\tau}} = \mu_g\left[\nabla\vec{u} - \frac{2}{3}\nabla\vec{u}\bar{\bar{I}}\right]$$

Porous media source term (7)

$$\vec{S}_{PM} = -\left(\frac{\mu_g\vec{u}}{K_{perm}} + K_{loss}\,\frac{1}{2}\,\rho_g u|u|\right)$$

$$K_{perm} = \frac{d_p^2}{150}\,\frac{\varepsilon^3}{(1-\varepsilon)^2}$$

$$K_{loss} = \frac{3.5}{d_p}\,\frac{(1-\varepsilon)}{\varepsilon^3}$$

Ergun equation (8)

$$\frac{\Delta p}{L} = \frac{150\mu_g}{d_p^2}\frac{(1-\varepsilon)^3}{\varepsilon^3}u + \frac{1.75\rho_g}{d_p}\frac{(1-\varepsilon)}{\varepsilon^3}u^2$$

Species diffusional transport (9)

$$\vec{J}_i = -\sum \rho_g D_i^{KT} \nabla Y_i \; - D_{i,T}^{KT}\frac{\nabla T}{T}$$

Three meshes of structured quadrilateral elements of various sizes are prepared for the grid independency study, performed according to Roache's Grid Convergence Index (GCI) based on the Richardson extrapolation.[46] The evaluated variable is the pressure drop over the HTK-S fixed bed reactor for a reactive calculation at a space time of 535 kgcat·s·$\mathrm{mol}_{\mathrm{CH_4}}^{-1}$ and a temperature of 723 K. The analysis uses an average order of convergence of 1.53 and a safety factor of 1.25. The results are listed in Table 3. The medium size grid comprising 701,250 cells is selected as the computational grid for the simulations because it provides good accuracy at a reasonable computational cost. The GCI results of the selected medium size-grid show $\mathrm{GCI}_{\text{fine-medium}}$ and $\mathrm{GCI}_{\text{medium-coarse}}$ values of 0.12% and 0.28%, respectively. The latter indicates that the calculation results using the medium grid are within the asymptotic range of convergence.

Table 3. Results of grid independent study

Grid	Total number of cells	Pressure drop (kPa)
Coarse	252,450	94.76
Medium	701,250	95.04
Fine	1,374,450	95.17

3.2. Methane catalytic oxidation model

The reaction equation for the total oxidation of methane over βCD-Cu/HAP reads:

$$CH_4 + 2\,O_2 \rightarrow CO_2 + 2\,H_2O \tag{10}$$

Several researchers already used a power law kinetic model as a first approximation to estimate VOC oxidation rates.[11, 15, 17, 47]

The power law reaction rate for methane oxidation reads: (11)

$$r = k\, p_{CH_4}^{m}\, p_{O_2}^{n}$$

with a rate constant equation (Arrhenius equation):

$$k = A\, exp\left(-\frac{E_{act}}{R_{gas}\, T}\right) \tag{12}$$

The partial reaction order of methane, m, and oxygen, n, is 0.61 and 0.09, respectively.[48] The pre-exponential factor, A, has a value of 578 mol·kgcat^{-1}·s^{-1}·kPa$_{\mathrm{CH_4}}^{-0.61}$·kPa$_{\mathrm{O_2}}^{-0.09}$,[48] and the apparent activation energy, E$_{act}$, is estimated to be 78 kJ·mol^{-1}.[48] The R$_{gas}$ refers to the universal gas constant, 8.314 J·mol^{-1}·K^{-1}.[48] This power law equation for methane oxidation is used as a kinetic model in the CFD calculations by implementing a User Defined Function (UDF).

4. Results and discussions

4.1. Parity plot and model validation

Figure 3 presents a parity plot that compares the experimental and simulated methane conversion, gathering the data obtained for all operating conditions. The figure includes two lines deviating from the first diagonal, set at ± 20%. The CFD model combined with power law kinetics is seen to approximate the experimental conversion of methane over a wide range of operating conditions with an average deviation of 17%.

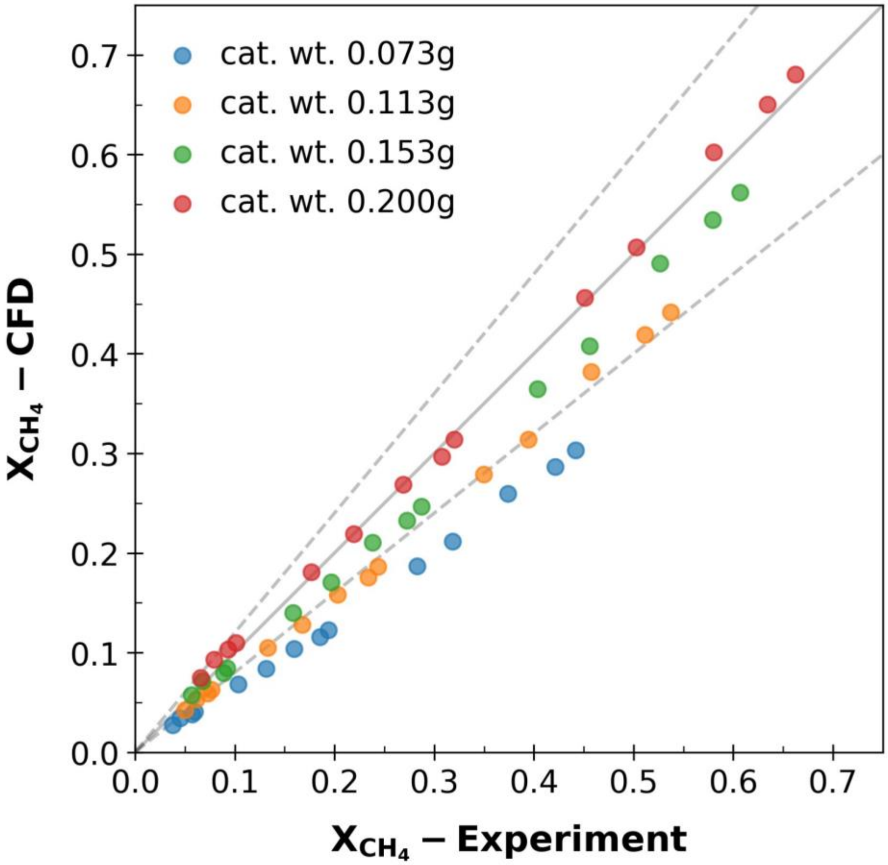

Figure 3. Parity plot for measured and calculated methane conversion at all operating conditions (including ± 20% deviation lines).

A quantitative agreement is obtained when the catalyst weight in the reactor amounts to 0.200 grams. With a catalyst weight of only 0.073 grams, the deviation between measured and calculated methane conversion exceeds 20% for most operating conditions, with a maximum of 38%. For a catalyst weight of 0.113 grams and 0.153 grams, the deviation reaches or exceeds up to 20% depending on the operation conditions. Based on the validated CFD model, the effects of operating conditions on the methane conversion are discussed specifically in the next section.

4.2. Effects of operating conditions on the methane conversion

4.2.a. Effect of methane inlet partial pressure on the methane conversion

Figure 4 compares the measured and simulated methane conversion in the fixed-bed reactor as a function of space time for inlet methane partial pressures of 2.91 kPa, 4.52 kPa, and 7.97 kPa. Data at temperatures of 623 K, 673 K, and 723 K are gathered. A changing methane partial pressure results in significant changes in the measured methane conversion. These changes are also captured in the calculated methane conversion due to the high partial order of methane in the power law kinetics, as demonstrated in Eq. 11.

An increase in the methane partial pressure reduces the methane conversion for all catalyst weights. For a specific catalyst weight, the methane partial pressure is increased while keeping the volumetric flow rate that enters the reactor at a constant value. Consequently, this adjustment reduces the space time value even though the amount of catalyst remains unchanged. The reduction of the space time at increasing methane partial pressure and constant catalyst mass is what causes the reduction of the methane conversion. The reduction of space time is observed in Figure 4, where the maximum value of the space time diminishes on the x-axis at increasing methane partial pressure. However, increasing the methane partial pressure also increases the reaction rate, as the power law model describes. The increase of methane partial pressure can increase the conversion when this occurs at a similar space time. To demonstrate it, 3 sets of experiments and simulations are done at comparable space time of 196 kgcat·s·$mol^{-1}_{CH_4}$ at increasing methane partial pressure; refer to Table S1 available in the Supporting information, by increasing methane partial pressure from 2.91 to 4.52 and to 7.97 kPa, the experimental methane conversion rises from 44% to 46% and to 50% while the simulated conversions shows an increase from 30% to 38% and to 51%.

For a given methane partial pressure and temperature, the methane conversion is seen to increase with increasing space time, that is with increasing weight of catalyst in the reactor. This increase becomes more significant with increasing temperature as the reaction rate increases (see Eqs. 11 and 12).

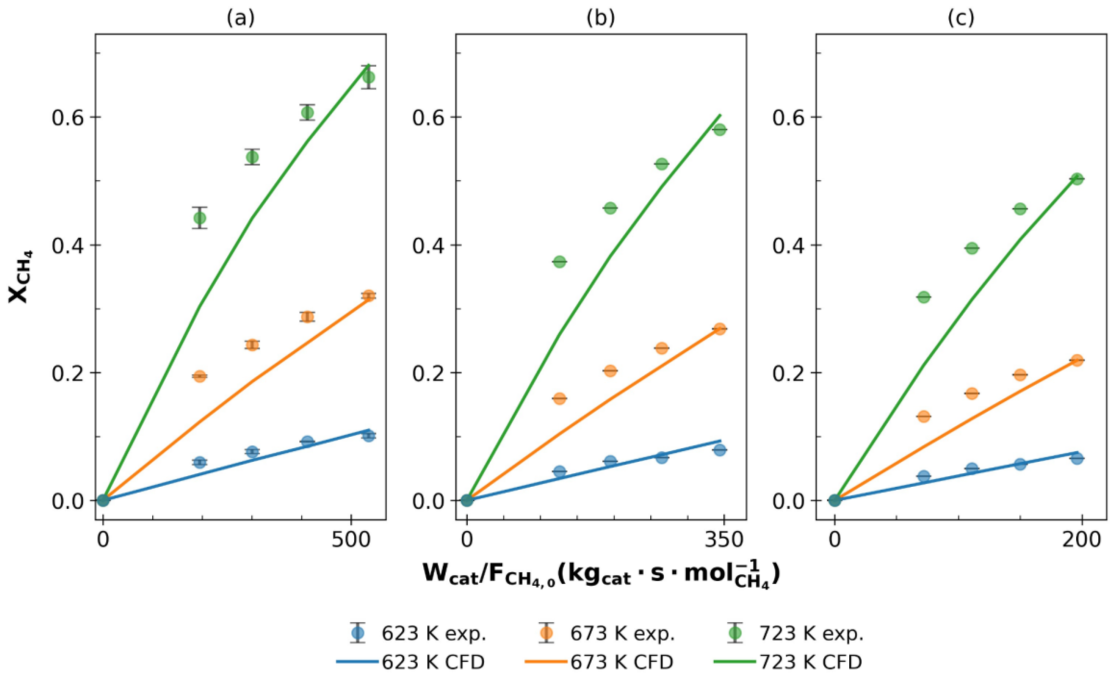

Figure 4. Methane conversion as a function of space time for methane inlet partial pressure of (a) 2.91 kPa (b) 4.52 kPa (c) 7.97 kPa. Oxygen partial pressure is 32.65 kPa.

The applied CFD model combined with the power law kinetic model qualitatively reproduces all measured data. A more quantitative agreement is obtained for all operating conditions at lower temperatures. As the temperature increases, the correspondence becomes more qualitative. This is possibly due to some of the assumptions made in the modeling. At all conditions, it is assumed that all particles are perfect spheres with a uniform diameter and that the bed has an isotropic porosity. In reality, the particles can be non-spherical[49] and they have a particle size distribution,[50] resulting in a non-uniform bed porosity.[51] These non-uniformities affect the bed hydrodynamics, such as the pressure and velocity fields, affecting the contact time between the gas and the catalyst and, thus, the reaction rate. In a 2D simulation of fixed-bed reactors, Jakobsen et al. found that pressure and velocity profiles are significantly affected when changing the radial bed porosity, while the influence on the reaction rate is relatively small.[52] From the results presented in this work, it must be concluded that the assumptions have a diminishing effect with decreasing temperature. As the temperature increases, the reaction rate and methane conversion increase, increasing the difference between the calculated and measured methane conversion. The latter is discussed in more detail in section 4.3.

4.2.b. Effect of oxygen inlet partial pressure on the methane conversion

Figure 5 shows the methane conversion as a function of space time for inlet oxygen partial pressures of 16.64 kPa and 32.65 kPa. Data are acquired at 623 K, 673 K, and 723 K. For a given oxygen partial pressure and temperature, the methane conversion increases as a function of space time, and the increase becomes more pronounced at higher temperature. Doubling the oxygen partial pressure increases the measured methane conversion only slightly, indicating a limited impact of the inlet oxygen partial pressure on the reaction rate. The calculated methane conversion remains nearly constant as well, corresponding to the low reaction order for oxygen in the power law rate equation (Eq. 11). In section 4.2.a, an increase in the methane partial pressure is observed to have a more significant effect on methane conversion.

The calculated methane conversions are in quantitative agreement with the experimental data at low operating temperatures. The agreement becomes more qualitative at high temperatures. These observations are in line with the results discussed in section 4.2.a. Similarly, the difference between the numerical result and the experimental value data decreases with increasing space time for all operating conditions.

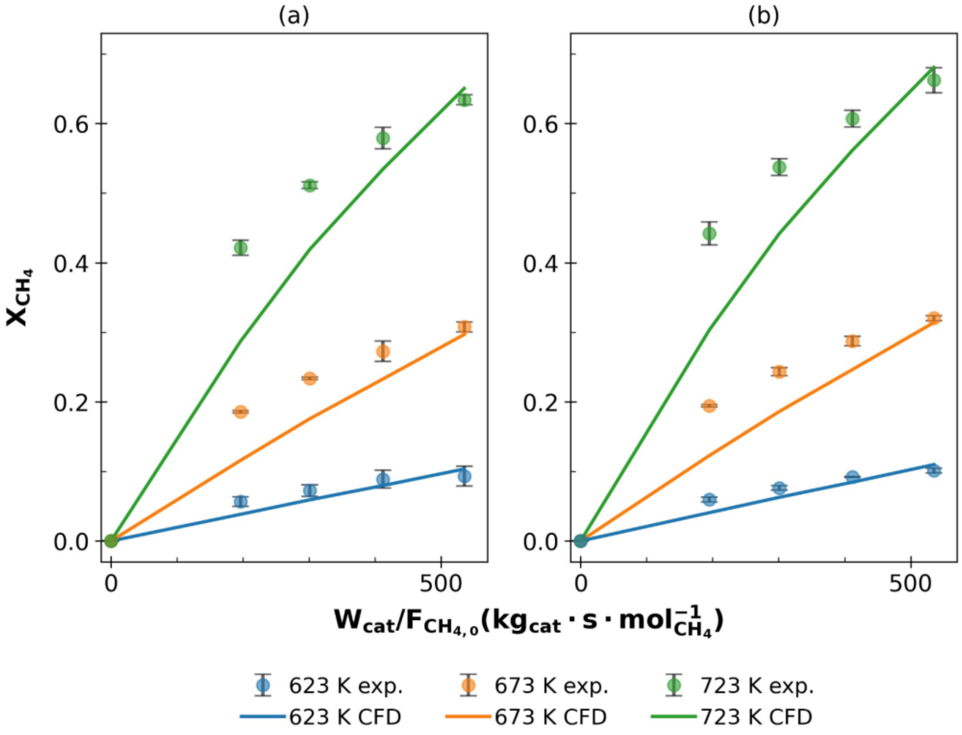

Figure 5. Methane conversion as a function of space time for oxygen inlet partial pressure of (a) 16.64 kPa (b) 32.65 kPa. Methane partial pressure is 2.91 kPa.

4.3. Use of a power law reaction model

From the parity plot in Figure 3, it is concluded that relatively high deviations between experimental and numerical methane conversions are obtained at low catalyst weights. The latter correspond to the lowest space times, where the measured methane conversion is between 5% and 45%. The observed deviations at these conditions are attributed to two factors: (1) the partial reaction orders m and n in the power law rate equation (Eq. 11) and (2) the impact of reaction products on the catalyst performance, i.e., on the reaction rate. Each factor is discussed in more detail in this section.

Heynderickx et al. reported that the partial reaction order for each reactant in the power law kinetic model will vary slightly depending on the temperature at which the experimental data are gathered and the regression is done.[17] For the oxidation of propane, another VOC, the partial reaction order of propane was found to vary slightly from 0.27 at 595 K to 0.21 at 648 K, while the partial reaction order of oxygen varies from 0.25 at 595 K to 0.22 at 648 K.[17] It is thus possible to improve the fitting of the model, specifically at low space time and high temperature, by changing the partial reaction orders. However, modifying the partial reaction order for methane oxidation from the initially reported values will reduce the model's prediction quality at other conditions.[48] Consequently, this observation is most likely not the main reason for the differences between experimental and numerical values at low space time.

The power law model calculates the reaction rate accounting for the methane and oxygen partial pressures only. However, the reaction products, CO_2 and water (see Eq. 10), could also influence the reaction rate. It was previously shown that water could play a role in catalytic processes by opening up a new reaction pathway with a low energy barrier.[53-54] For instance, an optimum amount of water molecules in the gas feed was found to improve the catalyst performance in the oxidative dehydrogenation of isobutyric acid.[53] Águila et al. reported that CO_2 in the gas phase does not affect the performance of a CuO catalyst used for methane oxidation.[16]

On the contrary, several works demonstrated that the excess presence of water could reduce the catalytic activity due to competitive adsorption on the catalyst surface. Ribeiro et al. observed a noticeable water inhibition effect on the total oxidation of methane over palladium catalysts.[55] Águila et al. also concluded that water inhibits total oxidation of methane when using CuO catalyst but also that the effect is reversible.[16] Similarly, Heyndericks et al. observed water's inhibitive effect when investigating the oxidation of propane over a CuO-CeO_2/γ-Al_2O_3 catalyst.[17] Excess water resulted in a competitive adsorption of propane and water on the active sites of the catalyst.[17]

The water inhibition effect is not captured by the power law model used here, as confirmed when comparing experimental and calculated data at high space time and high temperature. The experimental data presented in Figure 4 and Figure 5 learn that the methane conversion curve will reach a plateau value at even higher space times than the ones presented while the simulated methane conversion curve keeps rising almost linearly. Ultimately, a mechanistic model would unveil the role of water in greater detail and it would be the focus of our future work.

4.4. Reactor behavior insights

The numerical data obtained with the validated CFD model is now analyzed to provide insights into the behavior of the HTK-S reactor. Valuable information on concentration and temperature profiles inside the reactor is presented and discussed. Figure 6 shows the mole fraction distribution of all components (see Eq. 10) in the reaction zone at a space time of 535 $kg_{cat}\cdot s\cdot mol_{CH_4}^{-1}$ and a median temperature of 673 K. These conditions are selected since the methane conversion is close to the mean of the methane conversion range (4 – 66%), when operating at the highest catalyst mass (0.2 g catalyst). Partial pressures of 2.91 kPa for CH_4 and 16.64 kPa for O_2 are imposed in the gas feed flow. All species are found to have a linear concentration profile in the reaction zone. For the reaction products, the water concentration exceeds the CO_2 concentration. Under the assumption of competitive adsorption, this result may suggest that, potentially, water would impact the coverage of catalyst active sites, more than CO_2.[17] Although, the power law kinetic model used in this study disregards the impact of reaction products on the reaction rate, thus, further research is needed to draw a full conclusion on this hypothesis. As stated in Section 4.3, this is the focus of our future research. Sokhansanj et al. obtained similar linear concentration profiles when simulating a tubular fixed-bed reactor treating a diluted benzene and toluene gas stream with their CFD and ANN kinetic model.[19]

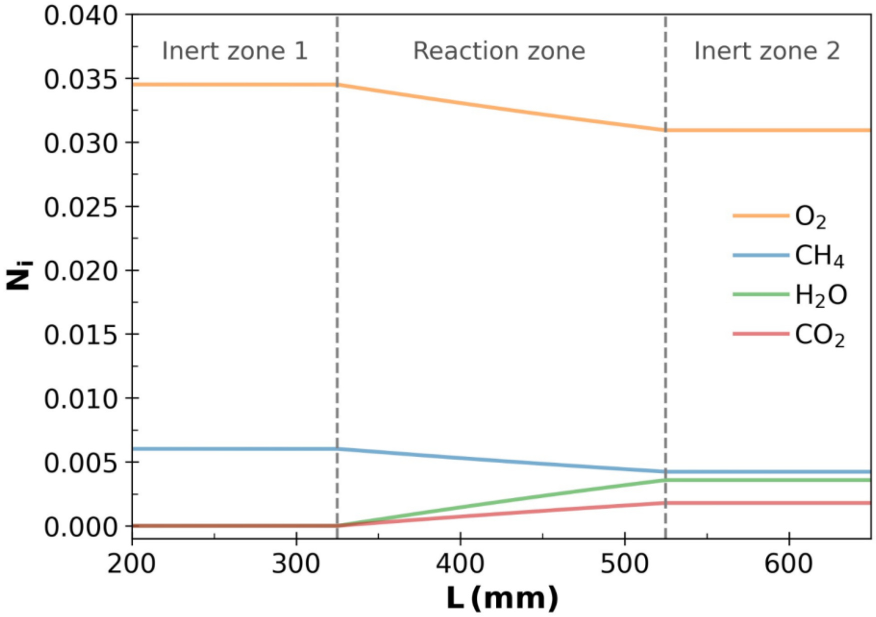

Figure 6. Species mole fraction distribution in the reaction zone at a space time of 535 $kg_{cat}\cdot s\cdot mol^{-1}_{CH_4}$ and a temperature of 673 K.

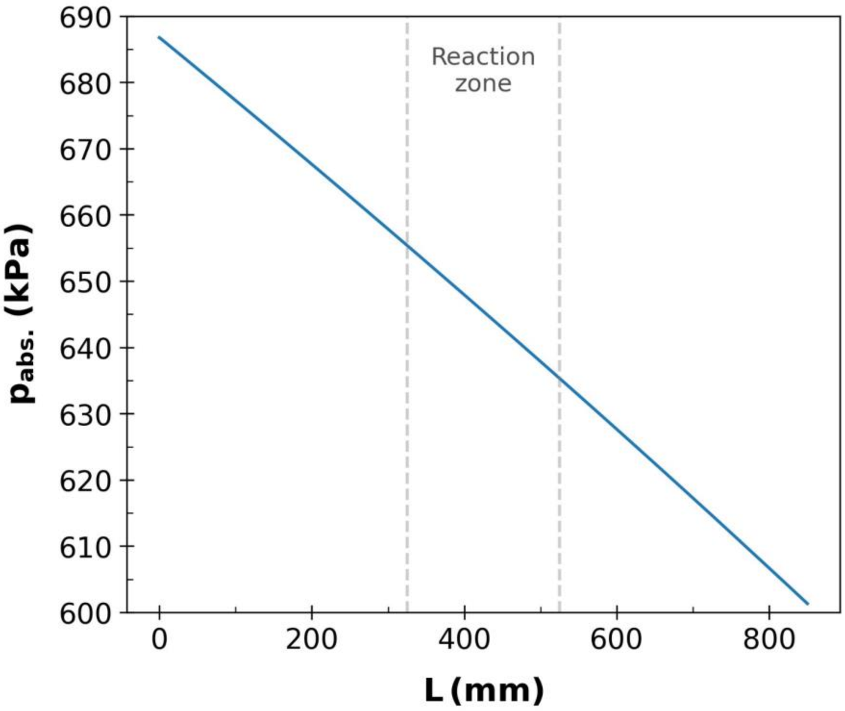

Figure 7. Absolute pressure distribution along the axial direction at a space time of 535 $kg_{cat}\cdot s\cdot mol^{-1}_{CH_4}$ and a temperature of 673 K.

The linear concentration profiles must be attributed to two observations. First, the reaction rate decreases with increasing axial reactor position as the reactants' concentration and the gas pressure decrease. Figure 7 depicts the pressure profile throughout the fixed-bed reactor along the axial direction. Even though the pressure drop throughout the total length of the reactor is substantial, the pressure drop throughout the reaction zone is merely 20 kPa. Second, the reactor is an isothermal reactor due to the significant methane dilution. As a result, the heat of reaction is minimal, and the gas temperature remains unaffected, as shown in Figure 8. The gas heats up rapidly at the reactor entrance due to the low mass flow rate and a (relatively) high amount of highly conductive inert material, α-Al_2O_3.

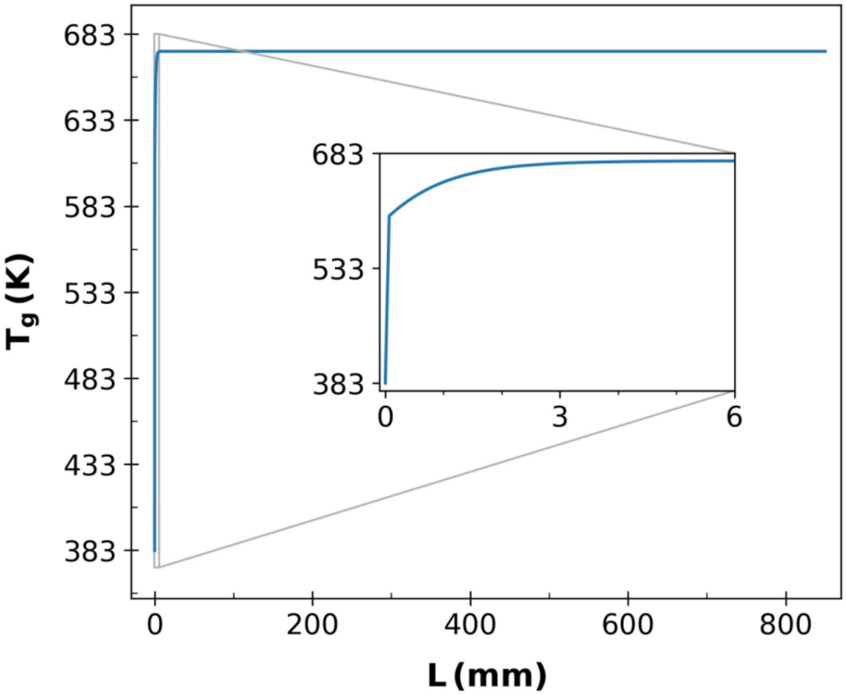

Figure 8. Temperature profile throughout the reactor at a space time of 535 kgcat·s·mol$^{-1}_{CH_4}$ and a temperature of 673 K (inset figure: zoomed in profile in the entrance of the reactor).

Radial distribution of temperature and methane mole fraction from the CFD calculation results are obtained at several axial directions throughout the reactor and shown in Figure 9 and Figure 10. The radial temperature distribution results support the assumption that a single temperature model is sufficient to simulate the HTK-S reactor. The gas temperature reaches the oven temperature at an axial distance of 5 mm from the reactor entrance (Figure 8). At that position the gas temperature is nearly constant along the reactor diameter as well. The small radial thermal effect in the reaction zone (325 – 525 mm) is a consequence of the high dilution of the VOC stream. These findings align with the work of Choudhury et al.[15] From Figure 10, it is concluded that the radial methane mole fraction distribution also appears linear throughout the reaction zone. The flat radial profile of the methane concentration explains the absence of radial temperature profile shown in Figure 9 due to the heavily diluted methane in the gas stream.

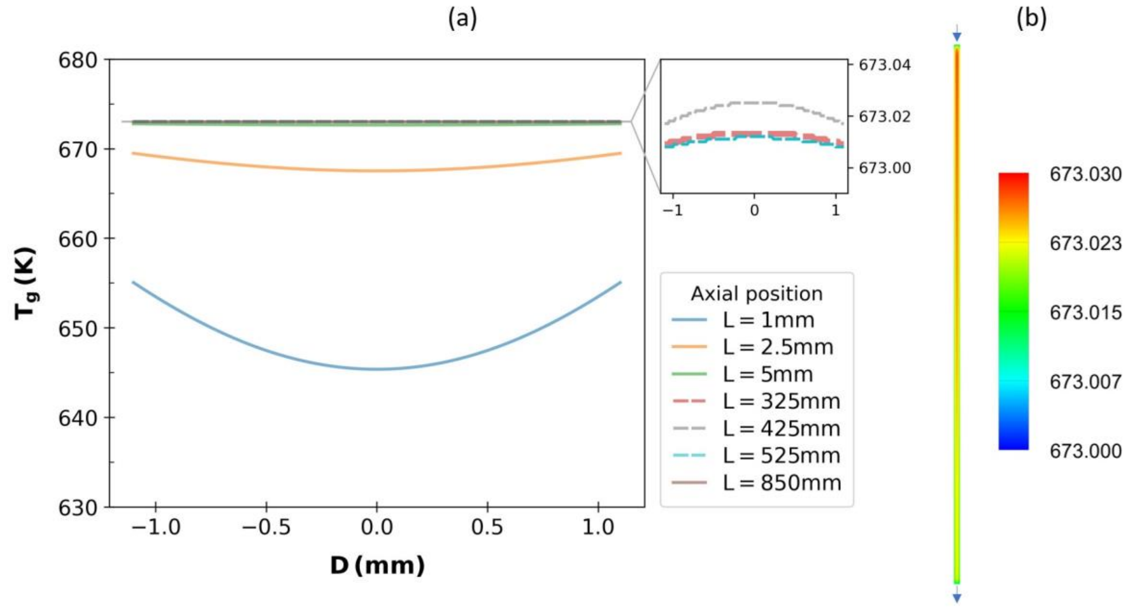

Figure 9. (a) Radial temperature distribution at several axial positions at a space time of 535 kgcat·s·$mol^{-1}_{CH_4}$ and a temperature of 673 K (inset figure: zoomed in distribution in the reaction zone) (b) simulated gas temperature contours in the reaction zone.

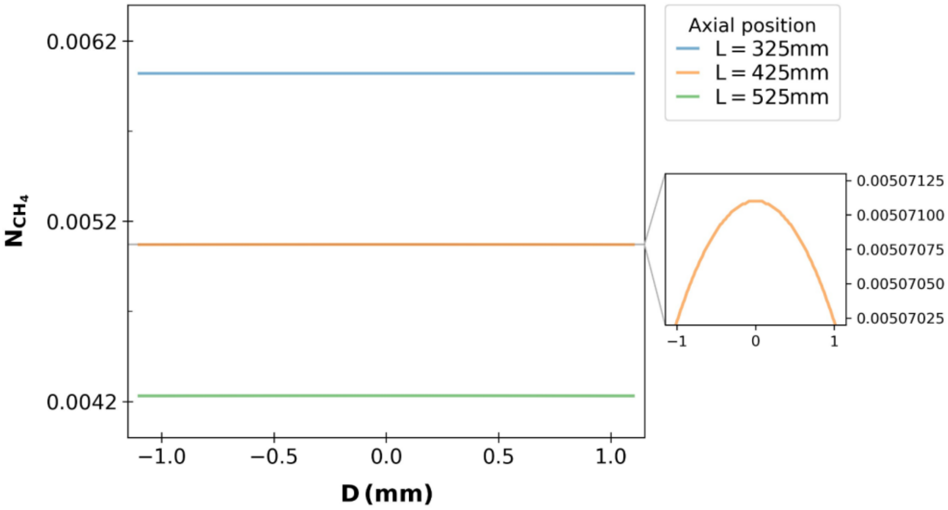

Figure 10. Radial methane mole fraction distribution at several axial positions in the reaction zone at a space time of 535 kgcat·s·$mol^{-1}_{CH_4}$ and a temperature of 673 K (inset figure: zoomed in distribution at the middle of the reaction zone).

The CFD flow field analysis results are able to provide information as a benchmark on the reactive information inside the fixed-bed reactor. Hence, a good understanding of the reactor behavior is obtained. Ultimately, these CFD analysis results suggest that conducting a simplified 1D reactor model to simulate the total oxidation of methane in the HTK-S reactor seems adequate.[56] The high length-to-diameter ratio of the reactor likely allows a simple plug-flow model to yield reasonable results. Therefore, the use of such model can be deployed in our future research.

5. Conclusions

Based on a porous media and power law kinetic model, a 2D reactive-flow CFD model is developed to simulate the catalytic oxidation of methane over a βCD-Cu/HAP catalyst in a fixed-bed reactor. The calculated methane conversion is in qualitative agreement with the experimental data obtained for different process parameters, including reaction temperature, catalyst weight, and partial pressure of methane and oxygen. It is observed that methane conversion increases with a rise in the reaction temperature and decreases with a rise in the methane partial pressure due to the decreasing space time, while the oxygen partial pressure has a limited influence.

A notable deviation between the numerical results and experimental data is repeatedly observed at lower space time, i.e., for the lowest catalyst weight. The power law kinetic model does not consider the effects of reaction products on the reaction rate, including a reduction of the catalyst's performance due to competitive adsorption between methane and the reaction products, water and CO_2. The discrepancy between the experimental and the numerical data can be attributed to the intensifying or inhibiting effect of the presence of water on methane conversion. In our future work, the focus will be to reveal the role of water in more depth. Based on the insights gained through the CFD analysis on the reactor behavior, a simplified 1D reactor model could be adequate to simulate the reactor. Accordingly, a simplified reactor model should be adopted in our future research with the HTK-S reactor.

Supporting information

Table with experimentally measured and CFD-calculated methane conversion values.

The Supporting Information is available free of charge via the Internet at https://pubs.acs.org/doi/10.1021/acs.iecr.3c03611.

Acknowledgment

This research has been funded by Ghent University (Belgium) through GOA project BOF19/GOA/003. The computational resources (Stevin Supercomputer Infrastructure) and services used in this work are provided by the VSC (Flemish Supercomputer Center), funded by Ghent University, FWO, and the Flemish Government – department EWI.

Conflict of Interest disclosure

The authors declare no competing financial interest.

Corresponding author

Geraldine J. Heynderickx - Laboratory for Chemical Technology, Department of Materials, Textiles, and Chemical Engineering, Ghent University, Technologiepark 125, B-9052 Ghent, Belgium; Email: Geraldine.Heynderickx@UGent.be; https://orcid.org/0000-0002-0713-9588

Authors

Mohammad Rusydi Fatahillah – Laboratory for Chemical Technology, Department of Materials, Textiles, and Chemical Engineering, Ghent University, Technologiepark 125, B-9052 Ghent, Belgium; https://orcid.org/0000-0002-1929-768X

Reza Monjezi – Laboratory for Chemical Technology, Department of Materials, Textiles, and Chemical Engineering, Ghent University, Technologiepark 125, B-9052 Ghent, Belgium; https://orcid.org/0000-0002-6797-4657

Yi Ouyang – Laboratory for Chemical Technology, Department of Materials, Textiles, and Chemical Engineering, Ghent University, Technologiepark 125, B-9052 Ghent, Belgium; https://orcid.org/0000-0002-1950-4538

Joris W. Thybaut – Laboratory for Chemical Technology, Department of Materials, Textiles, and Chemical Engineering, Ghent University, Technologiepark 125, B-9052 Ghent, Belgium; https://orcid.org/0000-0002-4187-7904

Dirk Poelman – LumiLab, Department of Solid State Sciences, Ghent University, Krijgslaan 281–S1, 9000 Ghent, Belgium; https://orcid.org/0000-0002-3930-172X

Funding Sources

This research has been funded by Ghent University (Belgium) through GOA project BOF19/GOA/003.

Nomenclature

A	Pre-exponential factor ($\mathrm{mol\cdot kg_{cat}^{-1}\cdot s^{-1}\cdot kPa_{CH_4}^{-0.61}\cdot kPa_{O_2}^{-0.09}}$)
C_p	Specific heat capacity ($\mathrm{J\cdot kg^{-1}\cdot K^{-1}}$)
d	Diameter (m)
D_i^{KT}	Mass diffusion coefficient for species-i ($\mathrm{m^2\cdot s^{-1}}$)
$D_{i,T}^{KT}$	Thermal diffusion coefficient for species-i ($\mathrm{m^2\cdot s^{-1}}$)
E	Total energy (J)

E_{act}	Apparent activation energy ($\text{J}\cdot\text{mol}^{-1}$)
$F_{CH_{4,0}}$	Initial molar flow rate of methane ($\text{mol}_{\text{CH}_4}\cdot\text{s}^{-1}$)
h	Enthalpy ($\text{J}\cdot\text{kg}^{-1}$)
h_i^f	Enthalpy of formation for species-i ($\text{J}\cdot\text{kg}^{-1}$)
I	Identity matrix (-)
J	Diffusion flux ($\text{kg}\cdot\text{m}^{-2}\cdot\text{s}^{-1}$)
K_{loss}	Inertial losses coefficient (m^{-1})
K_{perm}	Viscous resistance coefficient (m^{2})
k	Apparent rate constant ($\text{mol}\cdot\text{kg}_{\text{cat}}^{-1}\cdot\text{s}^{-1}\cdot\text{kPa}_{\text{CH}_4}^{-0.61}\cdot\text{kPa}_{\text{O}_2}^{-0.09}$)
L	Axial position, reactor length (m)
M	Molecular mass ($\text{kg}\cdot\text{kmol}^{-1}$)
N_i	Mole fraction for species-i (-)
p	Pressure (Pa)
R_{gas}	Universal gas constant ($\text{J}\cdot\text{mol}^{-1}\cdot\text{K}^{-1}$)
R_i	Reaction rate for species-i – FLUENT UDF ($\text{kmol}\cdot\text{m}^{-3}\cdot\text{s}^{-1}$)

r	Reaction rate – power law ($\mathrm{mol \cdot kg_{cat}^{-1} \cdot s^{-1}}$)
S_{PM}	Porous media source term ($\mathrm{kg \cdot m^{-1} \cdot s^{-2}}$)
T	Temperature (K)
u	Velocity ($\mathrm{m \cdot s^{-1}}$)
W_{cat}	Weight of catalyst (kg)
X_i	Conversion of species-i (-)
Y_i	Mass fraction of species-i (-)

Greek symbols

ε	Bed porosity (-)
λ	Thermal conductivity ($\mathrm{W \cdot m^{-1} \cdot K^{-1}}$)
μ	Viscosity (Pa·s)
ρ	Density ($\mathrm{kg \cdot m^{-3}}$)
τ	Stress tensor ($\mathrm{kg \cdot m^{-1} \cdot s^{-2}}$)

Abbreviations

ANN	Artificial neural network
CFD	Computational fluid dynamics

GCI	Grid convergence index
HAP	Hydroxyapatite
HTK-S	High-throughput kinetic screening
MOF	Metal organic framework
VOC	Volatile organic compound

Subscripts and superscripts

cat	Catalyst
f	Formation
g	Gas phase
i	Species-i
KT	Kinetic theory
m	Partial reaction order relative to CH_4
n	Partial reaction order relative to O_2
p	Particle
PM	Porous media
s	Solid phase
T	Thermal
0	Initial condition

References

(1) Brown, S. K.; Sim, M. R.; Abramson, M. J.; Gray, C. N. Concentrations of Volatile Organic Compounds in Indoor Air – A Review. *Indoor Air* **1994**, *4* (2), 123-134. DOI: 10.1111/j.1600-0668.1994.t01-2-00007.x.

(2) Jones, A. P. Indoor air quality and health. *Atmospheric Environment* **1999**, *33* (28), 4535-4564. DOI: 10.1016/S1352-2310(99)00272-1.

(3) Tham, K. W. Indoor air quality and its effects on humans—A review of challenges and developments in the last 30 years. *Energy and Buildings* **2016**, *130*, 637-650. DOI: 10.1016/j.enbuild.2016.08.071.

(4) Halios, C. H.; Landeg-Cox, C.; Lowther, S. D.; Middleton, A.; Marczylo, T.; Dimitroulopoulou, S. Chemicals in European residences – Part I: A review of emissions, concentrations and health effects of volatile organic compounds (VOCs). *Science of The Total Environment* **2022**, *839*, 156201. DOI: 10.1016/j.scitotenv.2022.156201.

(5) Kamal, M. S.; Razzak, S. A.; Hossain, M. M. Catalytic oxidation of volatile organic compounds (VOCs) – A review. *Atmospheric Environment* **2016**, *140*, 117-134. DOI: 10.1016/j.atmosenv.2016.05.031.

(6) Li, S.; Dang, X.; Yu, X.; Abbas, G.; Zhang, Q.; Cao, L. The application of dielectric barrier discharge non-thermal plasma in VOCs abatement: A review. *Chemical Engineering Journal* **2020**, *388*, 124275. DOI: 10.1016/j.cej.2020.124275.

(7) Hussain, M.; Russo, N.; Saracco, G. Photocatalytic abatement of VOCs by novel optimized TiO_2 nanoparticles. *Chemical Engineering Journal* **2011**, *166* (1), 138-149. DOI: 10.1016/j.cej.2010.10.040.

(8) Lou, B.; Shakoor, N.; Adeel, M.; Zhang, P.; Huang, L.; Zhao, Y.; Zhao, W.; Jiang, Y.; Rui, Y. Catalytic oxidation of volatile organic compounds by non-noble metal catalyst: Current advancement and future prospectives. *Journal of Cleaner Production* **2022**, *363*, 132523. DOI: 10.1016/j.jclepro.2022.132523.

(9) Khan, F. I.; Kr. Ghoshal, A. Removal of Volatile Organic Compounds from polluted air. *Journal of Loss Prevention in the Process Industries* **2000**, *13* (6), 527-545. DOI: 10.1016/S0950-4230(00)00007-3.

(10) Krishnamurthy, A.; Adebayo, B.; Gelles, T.; Rownaghi, A.; Rezaei, F. Abatement of gaseous volatile organic compounds: A process perspective. *Catalysis Today* **2020**, *350*, 100-119. DOI: 10.1016/j.cattod.2019.05.069.

(11) Gelles, T.; Krishnamurthy, A.; Adebayo, B.; Rownaghi, A.; Rezaei, F. Abatement of gaseous volatile organic compounds: A material perspective. *Catalysis Today* **2020**, *350*, 3-18. DOI: 10.1016/j.cattod.2019.06.017.

(12) Pang, C.; Han, R.; Su, Y.; Zheng, Y.; Peng, M.; Liu, Q. Effect of the acid site in the catalytic degradation of volatile organic compounds: A review. *Chemical Engineering Journal* **2023**, *454*, 140125. DOI: 10.1016/j.cej.2022.140125.

(13) Fiorenza, R. Bimetallic Catalysts for Volatile Organic Compound Oxidation. *Catalysts* **2020**, *10* (6), 661. DOI: 10.3390/catal10060661.

(14) Gao, Y.; Jiang, M.; Yang, L.; Li, Z.; Tian, F. X.; He, Y. Recent progress of catalytic methane combustion over transition metal oxide catalysts. *Frontiers in Chemistry* **2022**, *10*, 868-895, Review. DOI: 10.3389/fchem.2022.959422.

(15) Choudhary, V. R.; Deshmukh, G. M. Kinetics of the complete combustion of dilute propane and methyl ethyl ketone over Cr-doped ZrO_2 catalyst. *Chemical Engineering Science* **2005**, *60* (6), 1575-1581. DOI: 10.1016/j.ces.2004.10.028.

(16) Águila, G.; Gracia, F.; Cortés, J.; Araya, P. Effect of copper species and the presence of reaction products on the activity of methane oxidation on supported CuO catalysts. *Applied Catalysis B: Environmental* **2008**, *77* (3), 325-338. DOI: 10.1016/j.apcatb.2007.08.002.

(17) Heynderickx, P. M.; Thybaut, J. W.; Poelman, H.; Poelman, D.; Marin, G. B. Kinetic modeling of the total oxidation of propane over $CuO\text{-}CeO_2/\gamma\text{-}Al_2O_3$. *Applied Catalysis B: Environmental* **2010**, *95* (1), 26-38. DOI: 10.1016/j.apcatb.2009.11.018.

(18) Choi, B. S.; Yi, J. Simulation and optimization on the regenerative thermal oxidation of volatile organic compounds. *Chemical Engineering Journal* **2000**, *76* (2), 103-114. DOI: 10.1016/S1385-8947(99)00118-7.

(19) Sokhansanj, A.; Abdoli, S. M.; Zabihi, M. Insight into simultaneous catalytic oxidation of benzene and toluene in air over the nano-catalyst: Experimental and modeling via CFD-ANN hybrid method. *Process Safety and Environmental Protection* **2020**, *141*, 321-332. DOI: 10.1016/j.psep.2020.05.035.

(20) Niaei, A.; Salari, D.; Hosseini, S. A.; Nabavi, R.; Jodaei, A. CFD Simulation of Catalytic Oxidation of Ethyl Acetate over Cr-HZSM-5 Catalyst. *International Journal of Chemical Reactor Engineering* **2008**, *6* (1), 1-17. DOI: 10.2202/1542-6580.1679.

(21) Odiba, S.; Olea, M.; Hodgson, S.; Adgar, A.; Russell, P. Computational fluid dynamics in microreactors analysis and design: application to catalytic oxidation of volatile organic compounds. *Journal of Chemical Engineering & Process Technology* **2016**, *7*, 297-308. DOI: 10.4172/2157-7048.1000297.

(22) Ouyang, Y.; Heynderickx, G. J.; Van Geem, K. M. Development of intensified reactors: A process intensification methodology perspective. *Chemical Engineering and Processing - Process Intensification* **2022**, *181*, 109164. DOI: 10.1016/j.cep.2022.109164.

(23) Kulkarni, S. R.; Vandewalle, L. A.; Gonzalez-Quiroga, A.; Perreault, P.; Heynderickx, G. J.; Van Geem, K. M.; Marin, G. B. Computational Fluid Dynamics-Assisted Process Intensification Study for Biomass Fast Pyrolysis in a Gas–Solid Vortex Reactor. *Energy & Fuels* **2018**, *32* (10), 10169-10183. DOI: 10.1021/acs.energyfuels.8b01008.

(24) Vandewalle, L. A.; De, S.; Van Geem, K. M.; Marin, G. B.; Bos, R. Reactor Engineering Aspects of the Lateral Flow Reactor. *Industrial & Engineering Chemistry Research* **2020**, *59* (24), 11157-11169. DOI: 10.1021/acs.iecr.0c01229.

(25) Gao, X.; Zhu, Y. P.; Luo, Z. H. CFD modeling of gas flow in porous medium and catalytic coupling reaction from carbon monoxide to diethyl oxalate in fixed-bed reactors. *Chemical Engineering Science* **2011**, *66* (23), 6028-6038. DOI: 10.1016/j.ces.2011.08.031.

(26) Huang, K.; Lin, S.; Wang, J.; Luo, Z. Numerical evaluation on the intraparticle transfer in butylene oxidative dehydrogenation fixed-bed reactor over ferrite catalysts. *Journal of Industrial and Engineering Chemistry* **2015**, *29*, 172-184. DOI: 10.1016/j.jiec.2015.04.001.

(27) Borght, K. V. d.; Toch, K.; Galvita, V. V.; Thybaut, J. W.; Marin, G. B. Information-Driven Catalyst Design Based on High-Throughput Intrinsic Kinetics. *Catalysts* **2015**, *5* (4), 1948-1968. DOI: 10.3390/catal5041948.

(28) Ranga, C.; Lødeng, R.; Alexiadis, V. I.; Rajkhowa, T.; Bjørkan, H.; Chytil, S.; Svenum, I. H.; Walmsley, J.; Detavernier, C.; Poelman, H.; et al. Effect of composition and preparation of supported MoO_3 catalysts for anisole hydrodeoxygenation. *Chemical Engineering Journal* **2018**, *335*, 120-132. DOI: 10.1016/j.cej.2017.10.090.

(29) Berger, R. J.; Stitt, E. H.; Marin, G. B.; Kapteijn, F.; Moulijn, J. A. Eurokin. Chemical Reaction Kinetics in Practice. *CATTECH* **2001**, *5* (1), 36-60. DOI: 10.1023/A:1011928218694.

(30) Ibrahim, M.; Labaki, M.; Ponchel, A.; Giraudon, J.-M.; Gardoll, O.; Lamonier, J.-F. Beneficial Effect of β-Cyclodextrin Assisted Synthesis of CuO/Hydroxyapatite Catalyst in Toluene Oxidation. *ChemCatChem* **2023**, *15* (1), e202200943. DOI: 10.1002/cctc.202200943.

(31) Benyahia, F.; O'Neill, K. E. Enhanced Voidage Correlations for Packed Beds of Various Particle Shapes and Sizes. *Particulate Science and Technology* **2005**, *23* (2), 169-177. DOI: 10.1080/02726350590922242.

(32) Dixon, A. G.; Partopour, B. Computational Fluid Dynamics for Fixed Bed Reactor Design. *Annual Review of Chemical and Biomolecular Engineering* **2020**, *11* (1), 109-130. DOI: 10.1146/annurev-chembioeng-092319-075328.

(33) Zhuang, Y. Q.; Gao, X.; Zhu, Y. P.; Luo, Z. H. CFD modeling of methanol to olefins process in a fixed-bed reactor. *Powder Technology* **2012**, *221*, 419-430. DOI: 10.1016/j.powtec.2012.01.041.

(34) Lee, T. S.; Chung, J. N. Mathematical Modeling and Numerical Simulation of a Fischer–Tropsch Packed Bed Reactor and Its Thermal Management for Liquid Hydrocarbon Fuel Production using Biomass Syngas. *Energy & Fuels* **2012**, *26* (2), 1363-1379. DOI: 10.1021/ef201667a.

(35) Chen, X.; Dai, J.; Luo, Z. CFD modeling using heterogeneous reaction kinetics for catalytic dehydrogenation syngas reactions in a fixed-bed reactor. *Particuology* **2013**, *11* (6), 703-714. DOI: 10.1016/j.partic.2012.11.008.

(36) Hu, G.; Ye, Z.; Du, W.; Qian, F. CFD Simulation and Optimization of Gas-Solid Phase Temperature of Isothermal Acetylene Hydrogenation Reactor. *International Journal of Chemical Reactor Engineering* **2018**, *16* (5), 1-15. DOI: 10.1515/ijcre-2017-0220.

(37) Dixon, A. G.; Nijemeisland, M. CFD as a Design Tool for Fixed-Bed Reactors. *Industrial & Engineering Chemistry Research* **2001**, *40* (23), 5246-5254. DOI: 10.1021/ie001035a.

(38) Freund, H.; Zeiser, T.; Huber, F.; Klemm, E.; Brenner, G.; Durst, F.; Emig, G. Numerical simulations of single phase reacting flows in randomly packed fixed-bed reactors and experimental validation. *Chemical Engineering Science* **2003**, *58* (3), 903-910. DOI: 10.1016/S0009-2509(02)00622-X.

(39) Bai, H.; Theuerkauf, J.; Gillis, P. A.; Witt, P. M. A Coupled DEM and CFD Simulation of Flow Field and Pressure Drop in Fixed Bed Reactor with Randomly Packed Catalyst Particles. *Industrial & Engineering Chemistry Research* **2009**, *48* (8), 4060-4074. DOI: 10.1021/ie801548h.

(40) Pashchenko, D.; Karpilov, I.; Mustafin, R. Numerical calculation with experimental validation of pressure drop in a fixed-bed reactor filled with the porous elements. *AIChE Journal* **2020**, *66* (5), e16937. DOI: 10.1002/aic.16937.

(41) Jurtz, N.; Kraume, M.; Wehinger, G. D. Advances in fixed-bed reactor modeling using particle-resolved computational fluid dynamics (CFD). *Reviews in Chemical Engineering* **2019**, *35* (2), 139-190. DOI: 10.1515/revce-2017-0059.

(42) Ansys. *ANSYS Fluent User's Guide*; ANSYS, Inc, 2021.

(43) Ergun, S. Fluid flow through packed columns. *Chem. Eng. Prog.* **1952**, *48*, 89-94.

(44) Pavlišič, A.; Ceglar, R.; Pohar, A.; Likozar, B. Comparison of computational fluid dynamics (CFD) and pressure drop correlations in laminar flow regime for packed bed reactors and columns. *Powder Technology* **2018**, *328*, 130-139. DOI: 10.1016/j.powtec.2018.01.029.

(45) Romagnosi, L.; Gascoin, N.; El-Tabach, E.; Fedioun, I.; Bouchez, M.; Steelant, J. Pyrolysis in porous media: Part 1. Numerical model and parametric study. *Energy Conversion and Management* **2013**, *68*, 63-73. DOI: 10.1016/j.enconman.2012.12.023.

(46) Roache, P. J. Perspective: A Method for Uniform Reporting of Grid Refinement Studies. *Journal of Fluids Engineering* **1994**, *116* (3), 405-413. DOI: 10.1115/1.2910291.

(47) Heynderickx, P. M.; Thybaut, J. W.; Poelman, H.; Poelman, D.; Marin, G. B. Kinetic modeling of the total oxidation of propane over anatase and vanadia sputter deposited catalysts. *Applied Catalysis B: Environmental* **2009**, *90* (1), 295-306. DOI: 10.1016/j.apcatb.2009.03.020.

(48) Monjezi, R.; Bjelić, A.; Bitar, R.; Heynderickx, P.; Morent, R.; Thybaut, J. Abatement of VOCs : Kinetic Study of Methane Oxidation over Hydroxyapatite-Supported Catalysts. In 23rd Netherlands' Catalysis and Chemistry Conference (NCCC-XXIII) Noordwijkerhout, The Netherlands; 2022.

(49) Du, W.; Quan, N.; Lu, P.; Xu, J.; Wei, W.; Zhang, L. Experimental and statistical analysis of the void size distribution and pressure drop validations in packed beds. *Chemical Engineering Research and Design* **2016**, *106*, 115-125. DOI: 10.1016/j.cherd.2015.11.023.

(50) Caulkin, R.; Fairweather, M.; Jia, X.; Gopinathan, N.; Williams, R. A. An investigation of packed columns using a digital packing algorithm. *Computers & Chemical Engineering* **2006**, *30* (6), 1178-1188. DOI: 10.1016/j.compchemeng.2006.02.019.

(51) Hamzah, A. B.; Ookawara, S.; Yoshikawa, S.; Matsumoto, H. CFD modelling of mass and heat dispersion in sphere fixed bed with porosity-dependent segmented-continuum approaches. *Chemical Engineering Research and Design* **2019**, *141*, 93-114. DOI: 10.1016/j.cherd.2018.10.022.

(52) Jakobsen, H. A.; Lindborg, H.; Handeland, V. A numerical study of the interactions between viscous flow, transport and kinetics in fixed bed reactors. *Computers & Chemical Engineering* **2002**, *26* (3), 333-357. DOI: 10.1016/S0098-1354(01)00758-X.

(53) Vedrine, J. C.; Millet, J. M. M.; Volta, J. C. Molecular description of active sites in oxidation reactions: Acid-base and redox properties, and role of water. *Catalysis Today* **1996**, *32* (1), 115-123. DOI: 10.1016/S0920-5861(96)00185-X.

(54) Wang, C.; Gu, X. K.; Yan, H.; Lin, Y.; Li, J.; Liu, D.; Li, W. X.; Lu, J. Water-Mediated Mars–Van Krevelen Mechanism for CO Oxidation on Ceria-Supported Single-Atom Pt_1 Catalyst. *ACS Catalysis* **2017**, *7* (1), 887-891. DOI: 10.1021/acscatal.6b02685.

(55) Ribeiro, F. H.; Chow, M.; Dallabetta, R. A. Kinetics of the Complete Oxidation of Methane over Supported Palladium Catalysts. *Journal of Catalysis* **1994**, *146* (2), 537-544. DOI: 10.1006/jcat.1994.1092.

(56) Poissonnier, J.; Thybaut, J. W.; Marin, G. B. Understanding and optimization of chemical reactor performance for bimodal reaction sequences. *AIChE Journal* **2017**, *63* (1), 111-119. DOI: 10.1002/aic.15448.

Table of Contents/Abstract Graphics